# Unsteady Axial Mixing by Natural Convection in a Vertical Column

**M. H. I. Baird, K. Aravamudan, and N. V. Rama Rao**
Dept. of Chemical Engineering, McMaster University,
Hamilton, Ontario, Canada L8S 4L7

**J. Chadam and A. P. Peirce**
Dept. of Mathematics and Statistics, McMaster University,
Hamilton, Ontario, Canada L8S 4K1

*Unsteady axial mixing due to addition of a batch of sodium chloride solution at the top of a water-filled tube (2.63 cm i.d.) has been studied by measuring the developing concentration profile and the advancing front with dye added to the brine. Data have also been obtained with added baffle plates, with the use of a viscous aqueous solution, and in smaller diameter (1.48, 1.91 cm) tubes. Results can be approximately correlated by means of a model based on unsteady one-dimensional turbulent dispersion. Laminar flow affects the behavior of the advancing front at which the salt concentration is lowest.*

## Introduction

Axial mixing is important in the design of continuous reactors (Levenspiel, 1972) and countercurrent extraction columns (Pratt and Baird, 1983). The concept of an axial dispersion coefficient has been widely applied in modeling both of these types of equipment. The defining equation for the axial dispersion coefficient is analogous to Fick's Law for molecular diffusion. The flux due to axial dispersion is given by:

$$N = -E\frac{\partial c}{\partial z} \tag{1}$$

The values of $E$ are several orders of magnitude larger than molecular diffusion coefficients ($D$), because axial dispersion is caused by hydrodynamic rather than molecular behavior. In solvent extraction columns, axial dispersion in the continuous phase has been recognized as being due to a combination of factors, including:

- Turbulence, mainly due to agitation
- Circulation or flow nonuniformity, mainly due to the flow of dispersed droplets
- Axial transport in the wakes of droplets.

The interactions between these effects are quite complex; for example, increasing mechanical agitation can reduce circulation and therefore in some cases reduce the value of $E$. An early discussion of these effects is given by Rosen and Krylov (1974). Korchinsky (1988) has shown how wake transport effects are enhanced by mass transfer.

Recently Holmes et al. (1991) have pointed out an additional factor contributing to axial dispersion, namely natural convection. In general, the continuous phase in a counter-current extraction column will vary in density due to mass transfer. If the density increases with vertical height due to mass transfer, the potential exists for increased axial mixing due to natural convection. The conditions for continuous phase density to increase with height are satisfied by 4 combinations of column operating conditions and system properties, as listed in Table 1.

An increase of fluid density with height does not always result in instability. Taylor (1954) established the stability cri-

**Table 1. Conditions for Unstable Continuous Phase Density Gradients in Extraction Columns**

| Flow Direction of Cont. Phase | (type) | Mass-Transfer Direction $c$=Cont. $d$=disp. | Effect of Increasing Solute Conc. on Solution Density |
|---|---|---|---|
| Upward | I | $c \rightarrow d$ | reduces ($k<0$) |
| | II | $d \rightarrow c$ | increases ($k>0$) |
| Downward | III | $c \rightarrow d$ | increases ($k>0$) |
| | IV | $d \rightarrow c$ | reduces ($k<0$) |

terion for natural convection in a vertical tube, in terms of a critical density gradient:

$$\left(\frac{\partial \rho}{\partial z}\right)_c = 67.94\ D\ \mu/(g\ a^4) \tag{2}$$

This criterion was confirmed by Lowell and Anderson (1982) who measured the critical concentration gradients of sodium dichromate and mannose established in vertical capillary tubes with radius in the order of 1 mm. However typical calculations based on Eq. 2 show that the critical density gradients in a laboratory extraction column ($a = 2.5$ cm) would be extremely small and therefore would be exceeded in nearly all practical situations. The criterion of Eq. 2 is exceeded even more in the case of large diameter industrial columns operating under the conditions of Table 1. There is some evidence that axial mixing in extraction columns with mass transfer under the conditions of Table 1 exceeds the values measured by tracers in the absence of mass transfer (Bensalem, 1985; Dongaonkar et al., 1991). However, it is not easy to distinguish density gradient effects from other possible causes of increased axial mixing such as enhanced droplet coalescence or wake transport effects.

Holmes et al. (1991) and Baird and Rama Rao (1991) have measured axial mixing in specific relation to unstable density gradients in reciprocating plate columns of 7.6 and 5.1 cm diameter respectively. The gradients were maintained by passing a flow of light liquid up the column, and continuously feeding a denser (but miscible) stream near the top of the column, with the combined flows leaving the top of the column. The systems studied were brine/water and (cold water)/(hot water). The latter system was used in an insulated column to prevent heat loss effects. Axial dispersion coefficients were obtained by analysis of the measured steady state concentration or temperature profiles. It was found that in the absence of external agitation the effective axial dispersion coefficient was related to the density gradient by the equation

$$E = \ell^2 \left(\frac{g}{\rho} \cdot \frac{\partial \rho}{\partial z}\right)^{1/2} \tag{3}$$

where $\ell$ is a characteristic mixing length which is related to the column dimensions and geometry. The density term in the denominator of Eq. 3 can be approximated as the density of the pure solvent, $\rho_0$. Hence

$$E = \ell^2 \left(\frac{g}{\rho_0} \cdot \frac{\partial \rho}{\partial z}\right)^{1/2} \tag{3a}$$

In dilute systems the density is a linear function of concentration:

$$\rho = \rho_0 + kc \tag{4}$$

When Eqs. 1, 3a and 4 are combined, the flux is seen to vary with the 3/2 power of concentration gradient:

$$N = -\ell^2 \left(\frac{gk}{\rho_0}\right)^{1/2} \left(\frac{\partial c}{\partial z}\right)^{3/2} = -\alpha \left(\frac{\partial c}{\partial z}\right)^{3/2} \tag{5}$$

The term $\alpha$ is a constant for a given system and mixing length.

Equations 3a and 5 are applicable only when the density gradient is positive, that is when $k$ and the concentration gradient are of the same sign (see Table 1). In the reciprocating plate columns studied by Holmes et al. (1991) and Baird and Rama Rao (1991), the mixing length in the absence of agitation was 70% to 80% of the column diameter. As plate agitation was increased, the effective values of $E$ became less sensitive to the density gradient. A model based on energy dissipation due to natural convection and agitation was used by Holmes et al. (1991) to correlate their data and was further developed by Baird and Rama Rao (1991). Recently it has been found that natural convection has a significant effect under agitated, two-phase flow conditions (Aravamudan, 1992).

The above work was all carried out under steady state conditions. The present investigation examines the *unsteady* concentration profiles produced when a finite volume of a dense liquid (brine) is rapidly added at the top of a column containing a lighter liquid (water). This is analogous to the well known pulse tracer injection technique (Levenspiel and Smith, 1957) for studying axial mixing, with the novel feature that the "tracer" is deliberately made denser than the surrounding fluid so that buoyancy is the main cause of mixing. Previous workers have usually assumed that the tracer pulse has the same density as the surrounding liquid; this work will show that even a slight difference in density can have a strong effect on axial dispersion.

## Unsteady State Equations

The one-dimensional equation for accumulation of a solute is as follows:

$$\frac{\partial c}{\partial t} = -\frac{\partial N}{\partial z} \tag{6}$$

In the case of natural convection transport, the flux expression from Eq. 5 must be substituted, hence:

$$\frac{\partial c}{\partial t} = \alpha \frac{\partial}{\partial z}\left(\frac{\partial c}{\partial z}\right)^{3/2} \tag{7}$$

The boundary conditions are given by reference to Figure 1, which shows a semi-infinite tube extending from $z = 0$ to $z = -\infty$, with cross-sectional area A. Initially the tube is filled with pure solvent. At time $t = 0$ a finite amount $m$ of a denser solute is added, in very concentrated form, at position $z = 0$. (The analysis could equally well be carried out for a lighter solute added at the bottom of a semi-infinite tube extending upwards). A downwards convective flux occurs in accordance with Eq. 5 and the simplified boundary conditions for Eq. 7 are as follows:

$$t = 0,\ c = (m/A)\delta_0(z) \tag{8a}$$

$$z = 0,\ t > 0,\ \frac{\partial c}{\partial z} = 0 \tag{8b}$$

$$z = -\infty,\ t \geq 0,\ c = 0 \tag{8c}$$

where $\delta_0(z)$ is the Dirac delta function. The total amount of

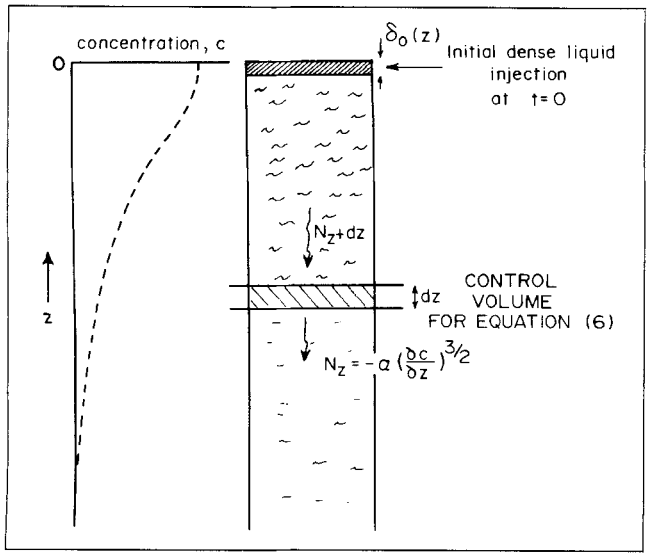


**Figure 1. Development of unsteady axial dispersion and typical concentration profile ($t>0$).**

tracer within the system at any time is related to Eq. 8a:

$$\int_{-\infty}^{0} c\,dz=\left(\frac{m}{A}\right)\int_{-\infty}^{0}\delta_0(Z)=\left(\frac{m}{A}\right) \tag{9}$$

By Lie group methods (Rogers and Ames, 1989), it can be shown that the only nontrivial solution for Eq. 7 has the form:

$$c(z,t)=t^p f(\xi) \tag{10}$$

where $\xi=z/t^q$.
The left-hand side of Eq. 7 is then written:

$$\frac{\partial c}{\partial t}=pt^{p-1}f-qt^{p-1}\xi f' \tag{11}$$

where prime denotes differentiation with respect to $\xi$.

For the right-hand side of Eq. 7, in cases where the concentration gradient is positive, we can write:

$$\left(\frac{\partial c}{\partial z}\right)^{3/2}=(t^{p-q}f')^{3/2} \tag{12}$$

and hence the right-hand side of Eq. 7 is:

$$\alpha\frac{\partial}{\partial z}\left(\frac{\partial c}{\partial z}\right)^{3/2}=\frac{3}{2}\alpha(t^{p-q}f')^{1/2}t^{p-2q}f''$$

$$=\frac{3}{2}\alpha t^{((3p-5q)/2)}(f')^{1/2}f'' \tag{13}$$

Equation 7 is now rewritten in terms of Eqs. 11 and 13:

$$t^{p-1}(pf-q\xi f')=\frac{3}{2}\alpha t^{((3p-5q)/2)}(f')^{1/2}f'' \tag{14}$$

If the solution for $f(\xi)$ is independent of time, then

$$p-1=(3p-5q)/2, \text{ hence } p=5q-2 \tag{15}$$

Equation 14 then reduces to:

$$(5q-2)f-q\xi f'=\frac{3}{2}\alpha(f')^{1/2}f'' \tag{16}$$

By taking $(5q-2)=-q$, one recovers the explicitly calculable solution commonly known as the Barenblatt solution (Barenblatt, 1952). Thus

$$q=1/3 \text{ and hence } p=-1/3 \tag{17}$$

Equation 16 becomes:

$$-(f+\xi f')/3=\frac{3}{2}\alpha(f')^{1/2}f'' \tag{18}$$

Simplifying,

$$(\xi f)'=-3\,\alpha((f')^{3/2})' \tag{19}$$

Integrating with respect to $\xi$:

$$\xi f'=-3\,\alpha(f')^{3/2}+k_1 \tag{20}$$

The integration constant $k_1$ is zero because of the boundary condition that $f'=0$ at $\xi=0$ (see Eq. 8b).

At this point it should be recalled from Figure 1 that the value of $z$ is zero or negative and hence $\xi$ is zero or negative. Fractional powers of $\xi$ will lead to complex numbers. Therefore further work will be carried out in terms of $(-\xi)$. From Eq. 20 with $k_1=0$,

$$f'=(-\xi f/3\alpha)^{2/3} \tag{21}$$

$$df/f^{2/3}=(-\xi)^{2/3}d\xi/(3\alpha)^{2/3} \tag{22}$$

Integrating,

$$3f^{1/3}=-(3/5)(3\alpha)^{-2/3}(-\xi)^{5/3}+k_2 \tag{23}$$

$$f(\xi)=[k_2/3-(1/5)(3\alpha)^{-2/3}(-\xi)^{5/3}]^3 \tag{24}$$

Substituting into Eq. 10 and defining $k_3$ as $k_2^3/27$, the concentration profile is:

$$c(z,t)=k_3t^{-1/3}[1-(1{,}125\;k_3\alpha^2)^{-1/3}(-\xi)^{5/3}]_+^3 \tag{25}$$

where $\xi=z/t^{1/3}$. The subscript + on the square bracket indicates that only the positive values apply; at large values of $(-z)$ such that the square bracket term is negative, $c=0$. This profile reaches a limiting value of 0 at a value of $z$ given by

$$z_o=-t^{1/3}(1{,}125\;k_3\alpha^2)^{1/5} \tag{26}$$

The profile Eq. 25 can also be written as:

$$c(z,t)=k_3t^{-1/3}[1-(z/z_o)^{5/3}]_+^3 \tag{27}$$

The constant $k_3$ can be evaluated from the condition that the mass of solute in the system is independent of time. The limit of Eq. 9 is changed from $-\infty$ to $-z_o$ and hence,

$$m/A = k_3 t^{-1/3} \int_{z_o}^{0} [1-(z/z_o)^{5/3}]^3 dz \tag{28}$$

This gives:

$$\begin{aligned} m/A &= -(125/312) k_3 t^{-1/3} z_o \\ &= -0.4006\ k_3 t^{-1/3} z_o \end{aligned} \tag{29}$$

Substituting for $z_o$ from Eq. 26 provides the following expression for $k_3$:

$$k_3 = 0.6646\ (m/A)^{5/6} \alpha^{-1/3} \tag{30}$$

Hence,

$$z_o = -3.756\ (m/A)^{1/6} (\alpha t)^{1/3} \tag{31}$$

and the concentration profile ($z_o < z < 0$) is given by:

$$\begin{aligned} c(z,t) = 0.6646\ &(m/A)^{5/6} (\alpha t)^{-1/3} \\ &\times [1-(-0.2662\ z (m/A)^{-1/6} (\alpha t)^{-1/3})^{5/3}]_+^3 \end{aligned} \tag{32}$$

The concentration tends to zero at a limiting value of $z$ given by Eq. 31. Equation 32 can also be expressed as:

$$c = 2.496\ (m/A z_o)[1-(z/z_o)^{5/3}]_+^3 \tag{33}$$

Equations 32 and 33 are based on an ideal Dirac pulse as given in Eq. 8(a). In practice such a pulse can only be approximated, and a numerical solution is required to check on the effect of the addition of a finite volume of concentrated salt solution at $z = 0$.

## Comparison of Numerical and Analytical Solution

In order to ensure the validity of the analytical method, the partial differential equation was solved numerically for the given boundary conditions using the finite difference explicit scheme. The difference equation corresponding to Eq. 7 is given below:

$$\frac{c_{i,j+1} - c_{i,j}}{\Delta t} = \frac{3}{2} (\ell)^2 \left( \frac{c_{i+1,j} - c_{i-1,j}}{2\Delta z} \right)^{1/2} \left( \frac{c_{i+1,j} - 2c_{i,j} + c_{i-1,j}}{\Delta z^2} \right) \tag{34}$$

This could be rewritten as follows:

$$c_{i,j+1} = c_{i,j} + \beta (c_{i+1,j} - c_{i-1,j})^{1/2} (c_{i+1,j} - 2c_{i,j} + c_{i-1,j}) \tag{35}$$

where

$$\beta = \frac{3}{2} \ell^2 \left( \frac{gk}{\rho} \right)^{1/2} \left( \frac{1}{2\Delta z^5} \right)^{1/2} \Delta t \tag{36}$$

The boundary conditions were chosen on the basis of the first spatial derivative vanishing at both ends of the column (implying zero flux at the ends). It was found during simulation that the concentrations at large distances were zero even for large values of $t$. (This verified the use of semi-infinite boundary conditions while solving the problem analytically.) Experience during simulation indicated that the scheme was stable when $\beta$ was less than unity. For a distance increment of 1 cm (a compromise between accuracy and time taken for simulation) and a mixing length arbitrarily chosen as 1.8 cm, this corresponds to a maximum time increment of 0.01 seconds. In order to make the comparison accurate the time increment was chosen as 0.001 s. If a distance increment of 0.1 cm had been chosen, the maximum time increment would have been $3 \times 10^{-5}$ s and computing requirements would have been prohibitive.

Computations for the case study in which 54 mL of the 100 g/L salt solution were added to a 2.63 cm diameter column were performed using VAX 8320 mainframe computer system. The CPU time taken for the longest (900 s) simulation was around 31 minutes. The concentration profiles from the simulation at all times were integrated and checked to confirm that the mass of tracer equaled that added initially. Double precision was used to avoid roundoff errors. The results are summarized in Table 2. The discrepancies could be attributed to numerical errors associated with the representation of the derivatives in the finite difference form. It can be concluded that the numerical and analytical calculations are in reasonable agreement for the case where 54 mL (a 10 cm layer) of concentrated salt was added at the top of the tube. Similar agreement was found when 5.4 mL (a 1 cm layer) of concentrated salt was added in the simulation.

**Table 2. Comparison Between Typical Numerically and Analytically Calculated Tracer Concentration Profiles**

| Position ($-z$) cm | $t = 33$ s | | $t = 100$ s | | $t = 300$ s | |
|---|---|---|---|---|---|---|
| | $c$ Num. | $c$ Analyt. | $c$ Num. | $c$ Analyt. | $c$ Num. | $c$ Analyt. |
| 0 | 46.08 | 47.10 | 32.19 | 32.55 | 22.41 | 22.57 |
| 5 | 43.99 | 44.39 | 31.39 | 31.53 | 22.10 | 22.18 |
| 10 | 38.92 | 38.86 | 29.38 | 29.39 | 21.32 | 21.36 |
| 15 | 32.33 | 31.88 | 26.63 | 26.53 | 20.23 | 20.23 |
| 20 | 25.12 | 24.39 | 23.42 | 23.22 | 18.91 | 18.88 |
| 25 | 18.06 | 17.16 | 19.95 | 19.68 | 17.42 | 17.36 |
| 30 | 11.75 | 10.84 | 16.41 | 16.10 | 15.80 | 15.72 |
| 35 | 6.66 | 5.86 | 12.98 | 12.64 | 14.12 | 14.01 |
| 40 | 3.04 | 2.47 | 9.79 | 9.45 | 12.40 | 12.28 |
| 45 | 0.94 | 0.64 | 6.97 | 6.65 | 10.70 | 10.57 |
| 50 | 0.11 | 0.04 | 4.60 | 4.32 | 9.05 | 8.92 |
| 55 | | | 2.73 | 2.51 | 7.48 | 7.35 |
| 60 | | | 1.39 | 1.23 | 6.03 | 5.90 |
| 65 | | | 0.55 | 0.46 | 4.70 | 4.58 |
| 70 | | | 0.13 | 0.09 | 3.54 | 3.43 |
| 75 | | | 0.01 | 0.00 | 2.54 | 2.45 |
| 80 | | | | | 1.72 | 1.45 |
| 85 | | | | | 1.08 | 1.01 |
| 90 | | | | | 0.60 | 0.56 |
| 95 | | | | | 0.28 | 0.25 |
| 100 | | | | | 0.10 | 0.08 |
| 105 | | | | | 0.02 | 0.01 |

Note: $c$ represents the concentration of tracer in grams/liter.

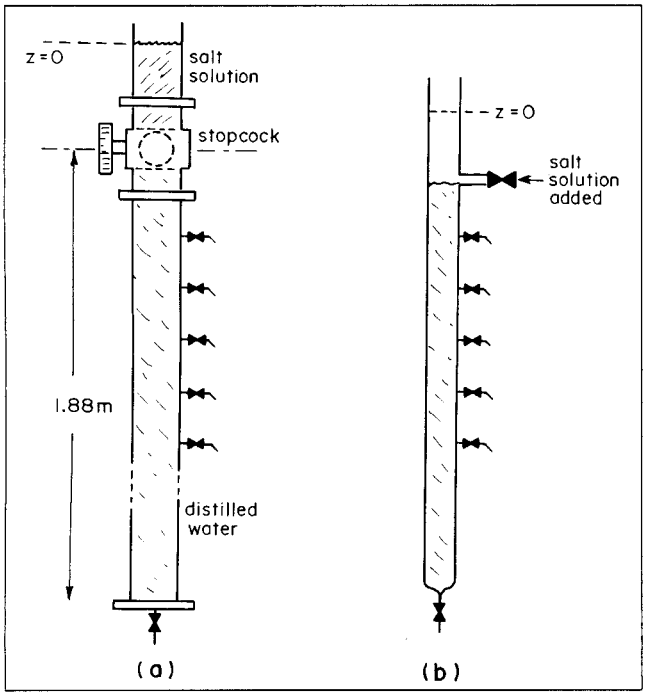


**Figure 2. Mixing tube apparatus.**

*(a) 2.63 cm i.d. (plastic); (b) 1.47 and 1.91 cm i.d. (glass).*

## Experimental

Unsteady convective mixing was investigated in carefully aligned vertical tubes of internal diameter 1.48, 1.91 and 2.63 cm. Most of the data were obtained with the 2.63 cm tube which is shown in Figure 2a. It was made of acrylic plastic and fitted at the top with a large plastic stopcock; the center of the stopcock was 1.88 m above the base of the tube. The opening of the stopcock was bored out to exactly the same diameter as the tube. Liquid sample ports were provided below the stopcock, with the first one located 22 cm beneath the stopcock centerline and lower ones positioned at 30.5 cm intervals.

At the beginning of an experiment, the tube was filled with distilled water above the level of the stopcock which was then closed. Distilled water remaining above the stopcock was removed by siphon tube. Then a known volume (usually 50 mL) of concentrated sodium chloride solution (typically 100 g/L) was added above the stopcock. Unsteady mixing was started by fully opening the stopcock so the dense concentrated salt solution could mix freely with the water below. The initial brine-water interface was nominally located at the upper end of the rotating cylindrical section. After a measured time, one of the sample ports was opened and about 10 mL of the solution was withdrawn. The sample was analyzed by electrical conductivity measurement which enabled salt concentration to be estimated with a precision of 0.05 g/L.

Only one salt sample was obtained in each experiment because the withdrawal of one sample had an effect on the developing profile. Thus for each measured time, the measurement of the complete concentration profile required up to six experiments with fresh water and sodium chloride solutions. The position $z=0$ was taken as the liquid surface after salt injection, as shown in Figure 1. Profiles were obtained for elapsed times between 33 s and 900 s. Conditions were generally such that the salt did not penetrate to the base of the tube, so the semi-infinite boundary condition of Eq. 8b was preserved.

**Table 3. Physical Properties of Liquid Systems**

| Liquid | Distilled Water | Aqueous Glucose/ Syrup Solutions |
|---|---|---|
| Density $\rho_o$, kg/m$^3$ | 997 | 1,227–1,240 |
| Viscosity $\mu$, mPa·s | 1.0 | 10.8–10.9 |
| Density Coeff. $k$ for Sodium Chloride | 0.70 | 0.54 |

Salt concentration profiles in the 2.63 cm tube were also measured in the presence of a stack of perforated plates. These stainless steel plates are of the type used in a pilot-scale Karr reciprocating plate extraction column (Otto H. York Co., Parsippany, NJ) and had the following dimensions: outer diameter, 2.54 cm; perforation diameter, 0.9 cm; thickness, 1 mm; fractional open area, 0.56. The plates were strung on a 6 mm diameter central rod at spacings of either 2.65 cm or 5.15 cm.

The smaller diameter tubes (1.47 cm and 1.91 cm) were made of glass (100 cm length) and are shown in Figure 2(b). No stopcocks were provided, so the procedure for adding the salt solution differed from that with the 2.63 cm tube. Initially the glass tube was filled with distilled water up to a side-arm about 10 cm beneath the top of the tube. Then an aliquot of salt solution, typically 10 mL of 100 g/L solution, was added at the side-arm over a period not exceeding 2 s. Mixing was allowed to proceed and after a measured time a few mL of solution was withdrawn from one of the lower sample ports (spaced at 15 cm intervals) for conductivity analysis. As in the case of 2.63 cm tube, the concentration profile at a given time was obtained by repeated experiments with fresh solution.

Table 3 summarizes the relevant properties of the salt/distilled water system. Some additional data were obtained with aqueous glucose or corn syrup solutions in order to examine the effect of viscosity. In making up these solutions the composition was adjusted to give a viscosity of 10.8 to 10.9 mPa·s, with density in the range 1,227 to 1,240 kg/m$^3$ in the salt-free solution. The dense tracer was a solution of sodium chloride in the viscous aqueous solution. The tracer solution had substantially the same viscosity as the salt-free solution. Conductivity analysis for sodium chloride concentration was again used, with an appropriate recalibration for the viscous solutions. Physical properties of the viscous system are summarized in Table 3.

## Results and Discussion

### *Brine-water system in 2.63 cm tube*

Figure 3 shows a typical set of salt concentration profiles at different elapsed times. Equation 32 has been fitted to the data using a mixing length $\ell=2.5$ cm corresponding to $\alpha=163.8\ \mathrm{g^{-1/2}\cdot cm^4\cdot s^{-1}}$. The data are fitted quite well except for the points nearest the origin. The deviations are far greater than the few percent which might be expected from the Dirac approximation (see Table 2 and preceding discussion.) There is also some deviation at the tail of the profiles, although this is not very apparent on a linear plotting scale. It was found

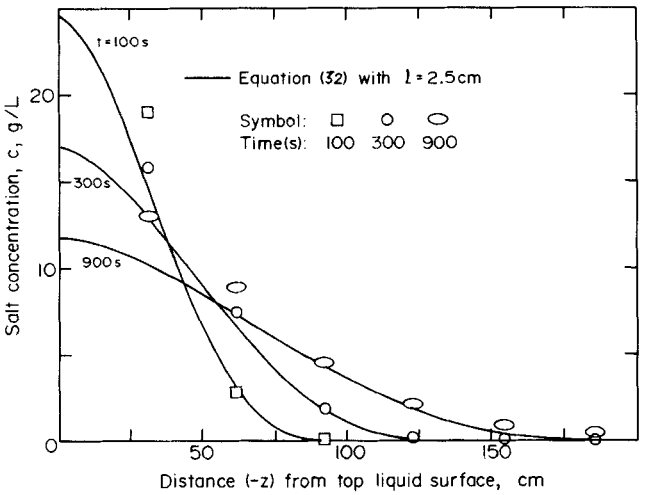


**Figure 3. Typical salt concentration profiles after addition of 50 mL of 100 g/L sodium chloride.**

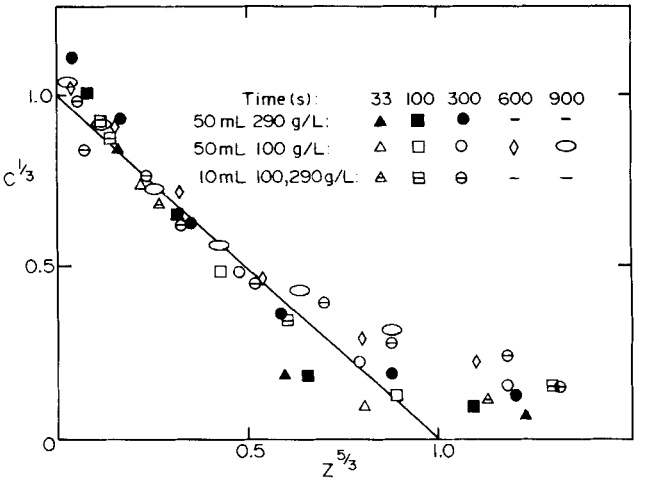


**Figure 4. Dimensionless concentration $C$ and dimensionless distance $Z$ plotted for various times and salt loadings in open 2.63 cm i.d. tube, water-based system.**

Assumed mixing length: 2.5 cm. Line represents Eq. 39.

that a reduction in the assumed mixing length would bring the points at the left of Figure 3 into line with the profiles, but then the other points did not fall on the calculated profiles; therefore the selected value of 2.5 cm for the mixing length was believed to be reasonable.

Equation 33 can be made dimensionless by introducing the dimensionless concentrations and distances:

$$C = cz_o/(2.496m/A) \tag{37}$$

$$Z = z/z_o \tag{38}$$

Furthermore the profile equation can be linearized by taking the 1/3 power of each side of Eq. 33 so that:

$$C^{1/3} = (1 - Z^{5/3})_+ \tag{39}$$

Thus when data for different elapsed times $t$ and tracer loadings $m/A$ are plotted as $C^{1/3}$ vs. $Z^{5/3}$ they should ideally fall on a single straight line with a slope of $-1$. The only adjustable parameter is the mixing length $\ell$.

Figure 4 shows a plot of this type for values of $t$ between 33 s and 900 s and for several different loadings ($m/A$). It is seen that the data points at intermediate values of $Z$ satisfy Eq. 39 quite well, but at low values of $Z$ there is significant positive deviation. However the deviation is smaller where only 10 mL of tracer were used (cross-bar symbols). The deviation at low $Z$ is therefore connected in some way with the larger volumes of tracer, but as already discussed (Table 2) it is not accounted for by the Dirac simplification. It could be due to some sort of response lag when the finite volume of dense fluid is initially released above the light liquid. Further discussion is provided at a later stage in this article.

Figure 4 also shows that as $Z$ approaches unity the concentrations become scattered and tend to exceed Eq. 39. The scatter is to be expected because of the poorer experimental precision of measuring $c$ for very dilute salt solution. For example at $C^{1/3} = 0.1$ the concentration is 1/1,000 of that at $z = 0$. Nevertheless it is significant that salt is detected at values of $Z$ in excess of unity. The mechanism for this apparent enhancement of mixing under very dilute conditions is also considered further at a later stage in this article.

The effect of adding stainless steel baffle plates on a central support rod is shown in Figure 5. The linearized profiles show the same trends as on Figure 4; the best agreement with the model equation occurs at intermediate values of $Z$. The fitted mixing length with a plate spacing of 5.15 cm is the same as for the open tube (Figure 4) but at a plate spacing of 2.65 cm the mixing length is reduced to 2.2 cm.

### *Brine-water system in 1.48 and 1.91 cm tubes*

Figure 6 shows the dimensionless linearized plot of salt con-

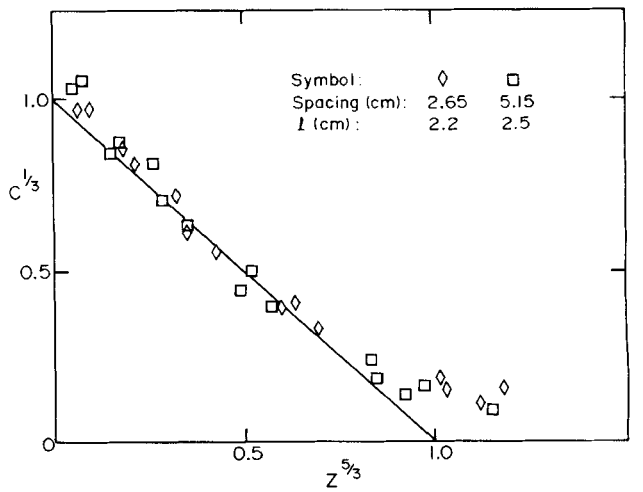


**Figure 5. Dimensionless concentration $C$ and dimensionless distance $Z$ plotted for times 33 to 600 s and 50 mL of 100 g/L sodium chloride added to baffled 2.63 cm i.d. tube, water-based system.**

Line represents Eq. 39.

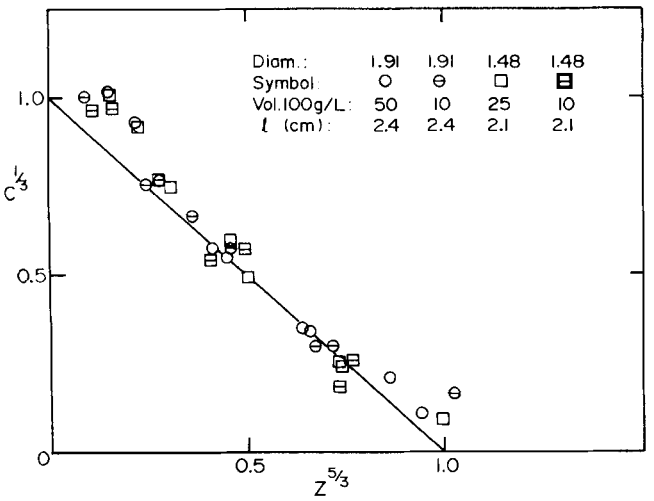


**Figure 6. Dimensionless concentration *C* and dimensionless distance *Z* plotted for open 1.48 and 1.91 cm i.d. tubes, water-based system.**

Elapsed times 50 and 100 s. Volumes of 10, 25 or 50 mL of 100 g/L sodium chloride added. Line represents Eq. 39.

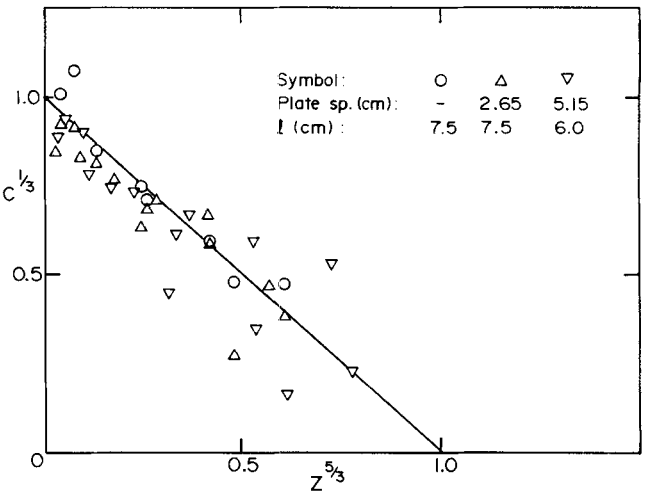


**Figure 7. Dimensionless concentration *C* and dimensionless distance *Z* plotted for 2.63 cm i.d. tube, glucose/syrup solutions, with and without baffles.**

Elapsed times 50, 150 and 300 s, with 50 mL of 100 g/L sodium chloride added. Line represents Eq. 39.

centration profiles for different times and loadings. The trends are similar to those described for the 2.63 cm tube (Figures 4 and 5). It is of particular interest that the fitted mixing lengths, based on the intermediate parts of the profile, are in excess of the tube diameter by 26% and 42% for the 1.91 and 1.48 cm tubes, respectively. In the unbaffled 2.63 cm tube the fitted mixing length was *5% less* than the tube diameter. Detailed discussion of the mixing lengths under different conditions will be given in a later section of the article.

### *Effect of increased viscosity on concentration profiles*

Data have been obtained for solutions of salt in aqueous glucose/syrup having the properties given in Table 3, using the 2.63 cm column. The linearized profiles in the absence of baffles, as represented by circle symbols in Figure 7, are fitted well by setting the mixing length $\ell$ as 7.5 cm. This value is *three times greater than* the one that fit the data for the water-brine system (Figure 4). When baffles are added with the viscous system, the profile points (triangles in Figure 7) become abnormally scattered and the mixing length estimates are very approximate. The scatter of the data is believed to be due to the nature of the flow through the baffles which could be observed as an intermittent streaming action through different perforations. As a result of this there was considerable radial nonuniformity in salt concentration. This nonuniformity fluctuated randomly with time and would lead to large variability in the salt concentrations measured in the samples taken at the wall of the column.

### *Mixing lengths from concentration profiles*

The mixing length values obtained from the salt concentration profiles (Figures 4 through 7) are summarized in Table 4.

Previous measurements of convection-driven mixing under steady state conditions (Holmes et al., 1991; Baird and Rama Rao, 1991) have indicated that in reciprocating plate columns of diameters 5.08 and 7.62 cm the mixing length is between 70% and 80% of the diameter in the absence of agitation. This work with the 2.63 cm column shows mixing lengths of 2.2 cm and 2.5 cm at respective plate spacings of 2.65 cm and 5.15 cm. These values are respectively 84% and 95% of column diameter.

The data for unbaffled columns of diameter 2.63, 1.91 and 1.48 cm show that the mixing lengths are respectively 95%, 126% and 142% of column diameter. Clearly a "similarity" approach based on local isotropic turbulence with the mixing length being proportional to column diameter is not appropriate in this range of column diameters. Moreover when a viscous solution is used with kinematic viscosity about 9 times greater than that of water, the apparent mixing length in the 2.63 cm diameter column is increased from 0.95 diameters to 2.85 diameters.

These effects of column diameter and liquid viscosity can be explained qualitatively by the increasingly laminar character of the mixing as viscosity is increased or column diameter is decreased. Large fluctuating striations ("fingers") were observed in the glucose solution, as opposed to smaller eddies in the aqueous system. The mixing length in the glucose/syrup system would approximate to the stable length of a striation which can readily exceed the column diameter. It is believed that the use of smaller columns with water would also have led to a more laminar type of behavior with increased radial nonuniformity, but this was hard to observe visually. Although

**Table 4. Mixing Lengths Obtained from Concentration Profiles**

| Column Dia. (cm) | 2.63 | | | | | 2.63 | 1.91 | 1.48 |
|---|---|---|---|---|---|---|---|---|
| System used* | *W* | *W* | *W* | *G* | *G* | *G* | *W* | *W* |
| Baffle Spacing (cm) | | | | | | | | |
| If Used | — | 5.15 | 2.65 | — | 5.15 | 2.65 | — | — |
| Mixing Length (cm) | 2.5 | 2.5 | 2.2 | 7.5 | 6.0# | 7.5# | 2.4 | 2.1 |

* *W* = aqueous, *G* = glucose/syrup solution
#approximate values

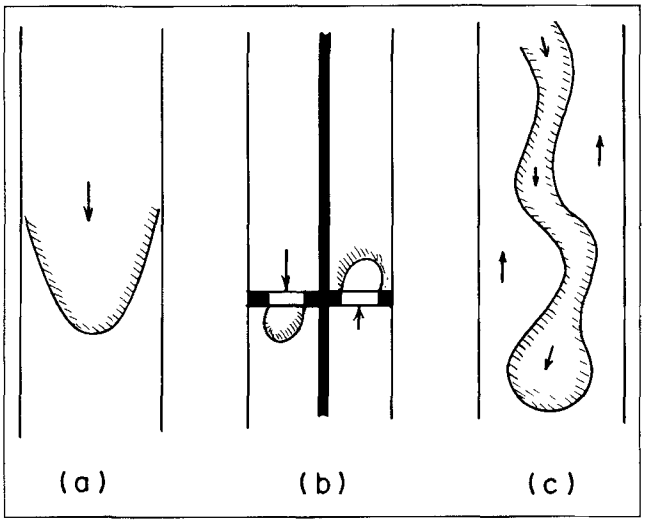


**Figure 8. Advancing front shapes in 2.63 cm i.d. tube.**

***(a) Open tube, water-based system; (b) Baffled tube, water-based system; (c) Open tube, glucose/syrup solutions.***

the mixing length is increased at higher viscosity because of the increased size of the striations, the form of Eq. 3 (and hence the profile equations) remains applicable because the fluid behavior is random and density-driven.

### *The advancing front*

According to Eqs. 32 and 33, the concentration profile spreads in the $(-z)$ direction and reaches $c=0$ at $z_o$ which is given by Eq. 31. As $z$ approaches $z_o$, the concentration according to Eq. 31 approaches zero asymptotically, that is to say the concentration gradient tends to zero; however it is physically unlikely that Eq. 3, which is based on a turbulent flow assumption, would remain valid at extremely small density gradients.

To examine the behavior of the advancing concentration front, flow visualization experiments were performed in the 2.63 cm tube. The procedure was similar to that already described except that a small concentration (about 1 g/L) of Rhodamine B red dye was dissolved in the concentrated salt solution before it was added at the top of the tube. The red color of this dye was so intense that the salt concentration front could be observed and videotaped for a long elapsed time after tracer addition.

In the case of the unbaffled tube with the water-based system, the falling dye-colored front appeared as a bullet-nose shape (Figure 8a) somewhat similar to that of a rising gas bubble in a vertical tube (Davies and Taylor, 1950). Although the front appeared quite smooth and laminar, turbulent eddies could be observed in the dye shortly above the front. In the presence of baffles the front appeared as an irregularly fluctuating sequence of plugs of liquid moving up as well as down through the perforations as sketched in Figure 8b. Motion above the front was essentially random. In the case of the viscous glucose/syrup solution the advancing front took the form of a long, snake-like striation or finger moving slowly down the tube as sketched in Figure 8c. The shape bore some resemblance to the laminar fingers of fluid that have been observed in fluid displacement in porous media (Homsy, 1987).

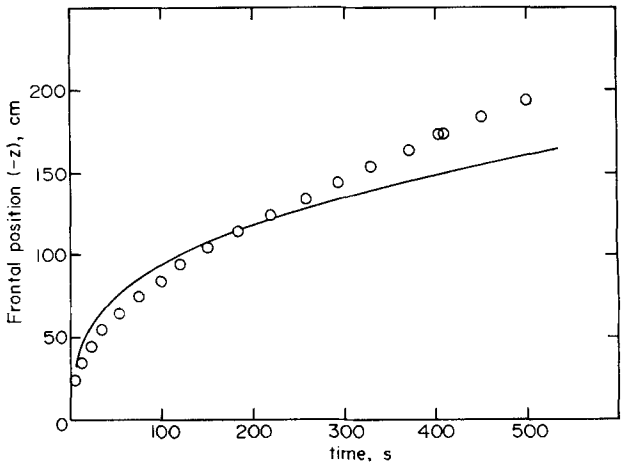


**Figure 9. Frontal position vs. time, open 2.63 cm dia. tube, water-based system.**

Tracer added: 50 mL of 100 g/L sodium chloride. Line represents Eq. 31 with $\ell = 2.5$ cm.

Although the radial position of the finger fluctuated randomly, the motion of fluid within the finger appeared to be laminar. Near the front there was little radial transport between the finger of salt solution and the surrounding salt-free liquid, but towards the top of the tube the motion became more disorganized.

Figures 9 and 10 show the position of the front in the tube as a function of time, for the water-based system in the absence of baffles. The datum $z=0$ was taken as the free surface of liquid as before. The curves represent the solution of Eq. 31 with the mixing length taken as 2.5 cm (see Figure 4). When 50 mL of 100 g/L sodium chloride are added (Figure 9) the observed movement of the frontal position $z$ as shown by the circle symbols is initially slower than the prediction from Eq. 31, but the data cross over the predicted curve at about 200 s. When only 10 mL of salt tracer is used (Figure 10) the same type of effect is seen with the crossover occurring at about

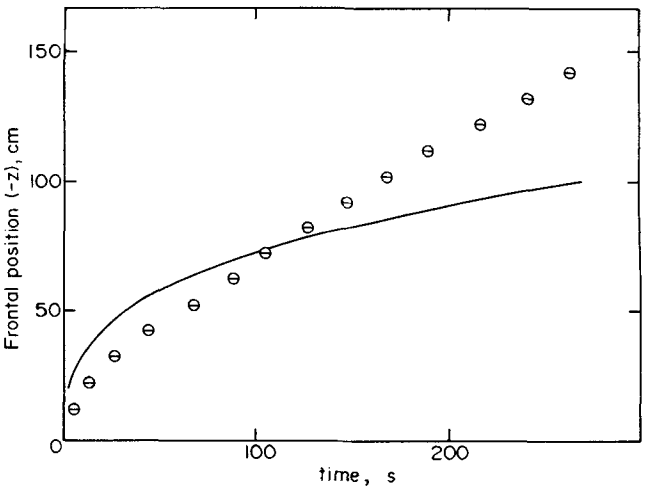


**Figure 10. Frontal position vs. time, open 2.63 cm dia. tube, water-based system.**

Tracer added: 10 mL of 100 g/L sodium chloride. Line represents Eq. 31 with $\ell = 2.5$ cm

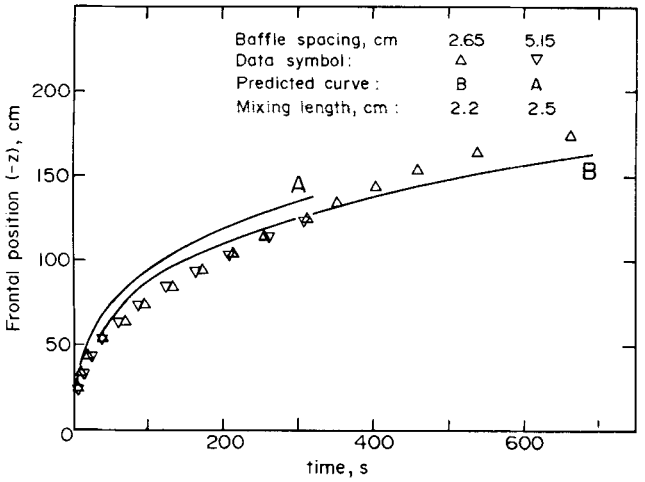


**Figure 11. Frontal position vs. time, baffled 2.63 cm dia. tube, water-based system.**

Tracer added: 50 mL of 100 g/L sodium chloride. Lines A and B represent Eq. 31 with mixing lengths as given above.

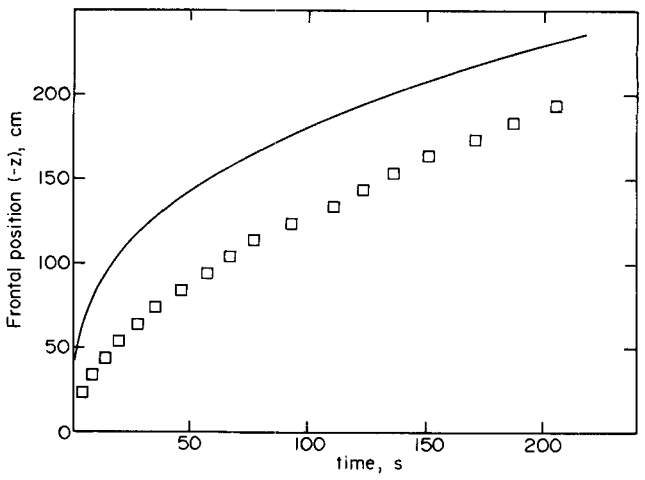


**Figure 12. Frontal position vs. time, open 2.63 cm dia. tube, glucose/syrup solutions.**

Tracer added: 50 mL of 100 g/L sodium chloride. Line represents Eq. 31 with $\ell = 7.5$ cm.

100 s in this case. For the more dilute system shown in Figure 10 it became impossible to identify the moving front after distances in excess of 140 cm due to the extreme dilution of the dye.

The initial movement of the fronts on Figures 9 and 10 is affected by two factors. First, the actual initial position of the front is at the stopcock (Figure 2) and not at the upper surface of the liquid ($z = 0$). In Figures 9 and 10 this position occurs at $(-z)$ values of 9.3 and 1.9 cm, respectively. This would seem to start the front at larger values of $(-z)$. However this effect is more than offset by the fact that the initial velocity is clearly much less than the very large value, tending to infinity as $t \to 0$, predicted according to Eq. 31. An order-of-magnitude estimate of the initial velocity can be made using the well-known equation of Davies and Taylor (1950) for the velocity of a cylindrical gas bubble in a vertical tube. In this work the equation must be adjusted to take account of the initial density difference between the salt solution and the water:

$$U = 0.35(g\ d\ \Delta\rho/\rho_o)^{0.5} \tag{40}$$

With an initial density difference $\Delta\rho$ of 70 kg/m$^3$, the initial velocity can be calculated as 4.7 cm/s. The average velocity of the front estimated from the data for the first 5 s in Figure 9 is 3.0 cm/s which is somewhat lower than the predicted 4.7 cm/s, but reasonable in view of rapid dilution of the salt solution after the stopcock is opened.

The initially slower spread of the salt compared with the turbulent model prediction explains why the concentrations within the profile are slightly higher than expected from Eq. 32 at small values of $z/z_o$ (Figures 3 to 7). As time elapses, the front position in Figure 9 approximates more closely to the values given by Eq. 31, but then after a long elapsed time the observed front position *exceeds* prediction. A qualitative explanation for this is that the laminar nature of the front allows significant radial nonuniformity and the "finger" of salt can advance faster through the fresh water than predicted from the turbulent model. This faster moving finger of very dilute salt explains how the concentration profile can extend beyond $z = z_o$ (Figures 4 to 7).

The presence of baffles (Figure 11) affects the advancing front in an interesting way; agreement with the turbulent model prediction for $z$ (Eq. 31) is considerably *better* than in the case of the unbaffled tube. This is particularly so at the closer baffle spacing used, 2.65 cm. It is believed that the alternating flow through the different perforations (Figure 8b) permits a faster initial spread of the dense salt and therefore a closer approach to turbulent conditions than the flow in an open tube. Also at high dilutions the formation of a single laminar finger is inhibited.

In the viscous system (Figure 12), the front position advances far more slowly than predicted and in fact it never catches up with the values of $z_o$ from Eq. 31. At short times the front velocity is significantly slower than the rate of change of $z$ predicted from the turbulent model. As discussed in connection with Figure 8c the simple turbulent mechanism is not applicable near the front, even though the profile data (Figure 7) can be fitted by choosing a large value of the "mixing length" in Eq. 39.

## Conclusions

Unsteady axial dispersion by natural convection after the addition of a batch of salt solution at the top of a column of water can be broadly described by a turbulence-based model. This is expressed as Eq. 7 and its analytical solution Eq. 32. The effective turbulent mixing lengths with aqueous solutions in open tubes of diameter 2.63, 1.92 and 1.48 cm are 2.5, 2.4 and 2.1 cm, respectively. The presence of perforated plate baffles in the 2.63 cm diameter tube has only a slight effect in reducing the mixing length. When a viscous aqueous solution of glucose/syrup is used, the effective mixing length is substantially increased and this is attributed to a laminar fingering process. Although the turbulent model cannot be expected to apply to such a process, the model equation can be fitted to the central part of the profile.

Measurements of the advancing front show that the tur-

bulent model expressed by Eq. 31 tends to overpredict the initial velocity of advance of the front, consistent with the observation that the profile is initially slower to spread than predicted. Conversely, after a long time the measured frontal velocity exceeds the prediction of Eq. 31 and the dilute salt solution is able to penetrate further than expected, due to a laminar fingering process. The frontal advance rate agrees most closely with the turbulent model when baffles are present in the tube.

These results are significant because they show that the "pulse tracer injection" method for studying axial mixing in a vertical column is very sensitive to a density difference between the tracer solution and the liquid. This sensitivity is likely to remain important even at very small density differences where the rate of spreading of the salt solution exceeds prediction by the turbulent model.

## Acknowledgments

The authors are grateful to the Natural Sciences and Engineering Research Council of Canada for financial support through an Operating Grant. They are also grateful to the Otto York Company for the loan of perforated plates. A presentation based upon this work has been made at the 42nd Canadian Chemical Engineering Conference, Toronto, October 1992.

## Notation

$a$ = radius of tube, m
$A$ = cross-sectional area of tube, $m^2$
$c$ = concentration, $kg/m^3$ or g/L
$C$ = dimensionless concentration, see Eq. 37
$d$ = diameter of tube, m
$D$ = molecular diffusivity, $m^2/s$
$E$ = axial dispersion coefficient, $m^2/s$
$f$ = function of $\xi$
$g$ = gravitational acceleration, $m/s^2$
$k$ = density coefficient, see Eq. 4
$k_1$ = integration constant in Eq. 20
$k_2$ = integration constant in Eq. 23
$k_3$ = $k_2^3/27$, see Eq. 25
$\ell$ = mixing length, m
$m$ = mass of salt in added solution, kg
$N$ = flux, $kg/(m^2s)$
$p, q$ = exponents, see Eq. 10
$t$ = time, s
$U$ = frontal velocity from Eq. 40, m/s
$z$ = axial distance, m
$z_o$ = value of $z$ at which $c=0$, see Eqs. 26 and 31
$Z$ = dimensionless distance, $z/z_o$

### Greek letters

$\alpha$ = coefficient in Eq. 5, $kg^{1/2}\cdot m^4/s$
$\beta$ = coefficient defined by Eq. 36
$\delta_0$ = Dirac delta function of $z$
$\Delta\rho$ = density difference, $kg/m^3$
$\rho_0$ = density in absence of salt, $kg/m^3$
$\rho$ = solution density, $kg/m^3$
$\mu$ = viscosity, Pa·s
$\xi$ = variable $z/tq$, see Eq. 10

### Subscripts

$i$ = denoting intervals of distance in $z$ direction
$j$ = denoting intervals of time

## Literature Cited

Aravamudan, K., unpublished data (1992).
Baird, M. H. I., and N. V. Rama Rao, "Axial Mixing in a Reciprocating Plate Column in Presence of Very Small Density Gradients," *AIChE J.*, **37**, 1091 (1991).
Barenblatt, G. I., "Some Unsteady Motions of Liquid or Gas in a Porous Medium," *Prikl Matematika i Mekanika (USSR)*, **16**, 67 (1952).
Bensalem, A., "Hydraulics and Mass Transfer in a Reciprocating Plate Column," Ph.D. Thesis, E. T. H. Zurich (1985).
Davies, R. M., and G. I. Taylor, "The Mechanics of Large Bubbles Rising Through Extended Liquids and Through Liquids in Tubes," *Proc. Roy. Soc. Ser. A.*, **200**, 375 (1950).
Dongaonkar, K. R., H. R. C. Pratt, and G. W. Stevens, "Mass Transfer and Axial Dispersion in a Kuhni Extraction Column," *AIChE J.*, **37**, 694 (1991).
Holmes, T. L., A. E. Karr, and M. H. I. Baird, "Effect of Unfavourable Continuous Phase Density Gradient on Axial Mixing," *AIChE J.*, **37**, 360 (1991).
Homsy, G. M., "Viscous Fingering in Porous Media," *Ann. Rev. Fluid Mech.*, **19**, 271 (1987).
Korchinsky, W. J., "A Dispersion-Entrainment Model for Liquid-Liquid Extraction Column Performance Prediction," *Chem. Eng. Sci.*, **43**, 349 (1988).
Levenspiel, O., *Chemical Reaction Engineering*, Ch. 9, 2nd edition, Wiley, New York (1972).
Levenspiel, O., and W. K. Smith, "Notes on the Diffusion Model for the Longitudinal Mixing of Fluids in Flow," *Chem. Eng. Sci.*, **6**, 227 (1957).
Lowell, M. E., and J. L. Anderson, "Stable Concentration Gradients in a Vertical Tube," *Chem. Eng. Commun.*, **18**, 93 (1982).
Pratt, H. R. C., and M. H. I. Baird, "Axial Dispersion," Ch. 6 in *Handbook of Solvent Extraction*, T. C. Lo, M. H. I. Baird, and C. Hanson, eds., Wiley, New York (1983).
Rogers, C., and W. F. Ames, *Nonlinear Boundary Value Problems in Science and Engineering*, Academic Press, New York (1989).
Rosen, A. M., and V. S. Krylov, "Theory of Scaling Up and Hydrodynamic Modelling of Industrial Mass Transfer Equipment," *Chem. Eng. J.*, **7**, 85 (1974).
Taylor, G. I., "Diffusion and Mass Transport in Tubes," *Proc. Phys. Soc., Sect. B*, **67**, 857 (1954).

*Manuscript received March 31, 1992, and revision received Aug. 10, 1992.*